J Mater Sci (2006) 41:4466–4476
DOI 10.1007/s10853-006-0092-x

Stress fields at boundaries between contacting particles

Anders Thölén

Received: 6 January 2006 / Accepted: 28 February 2006 / Published online: 29 June 2006

Abstract Small metal particles in the size range 0.1 μm sometimes exhibit stress fringes near the contacting boundary as observed in the transmission electron microscope. The possible causes for these stress fields are investigated in terms of different models: adhesion, external forces (possibly magnetic), dislocations in the grain boundary area or ''squeezed-in'' extra material in the grain boundary zone. In all these cases high stresses are expected near the contacting area. Adhesion between particles becomes more apparent the smaller they are and is thus very important in nanotechnology.

Background

In 1972 Easterling and Thölén [1] first reported about some stress fields which were observed at the contact between small particles extracted from a copper alloy containing coherent Fe–Ni particles (Fig. 1). This observation was explained in terms of adhesion between the particles. The surface energy of the system forced the particles together essentially in the same way as liquid drops amalgamate. The solid particles, however, only made contact across a small area rather than merge into one big particle.

The first theory to explain a similar phenomenon, the so called JKR-theory named after Johnson et al. [2], is based on an energy balance. The JKR-theory is an extension of Hertz' treatment [3], which describes what happens when two spheres in contact are subjected to an outside force pair, F, acting along the central line. The contact area then becomes finite (Fig. 2) with a radius which depends on the particle radius, the applied force and the elastic modulus of the particles.

$$a = \left(\frac{3(1-\nu^2)FR}{4E}\right)^{\frac{1}{3}}, \tag{1}$$

F = applied force (N), R = particle radius (m), a = radius of contact due to an applied force (m), E = modulus of elasticity (N/m^2), ν = Poisson's ratio.

When the applied force vanishes the contact radius drops to zero in Hertz' model. In the JKR-theory, on the other hand, a positive contact radius is obtained even if the applied force is zero. The surface energy of the system is driving the system towards an energy minimum in a similar way as water droplets attract each other to minimize the total energy.

By forming a finite contact radius between the two particles the outer surface area is diminished and a grain boundary with a certain energy is formed (Fig. 2). In the contact zone a stress field with a compressive zone in the centre and a tensile zone further out is built up.

The sum of the three energy terms, surface energy, grain boundary energy and stored elastic energy, has a minimum for a finite contact radius, a_{adh}.

$$\begin{aligned} \gamma_{\mathrm{eff}} &= 2\gamma_{\mathrm{s}} - \gamma_{\mathrm{gb}}, \\ a_{\mathrm{adh}} &= \sqrt[3]{\frac{9\pi}{4}\cdot\frac{(1-\nu^2)R^2}{E}\cdot\gamma_{\mathrm{eff}}}, \\ \sigma &= \frac{2Ea_{\mathrm{adh}}}{3\pi(1-\nu^2)R}\cdot\frac{2-3\frac{r^2}{a_{\mathrm{adh}}^2}}{\sqrt{1-\frac{r^2}{a_{\mathrm{adh}}^2}}}, \end{aligned} \tag{2}$$

A. Thölén (✉)
Department of Applied Physics, Microscopy and Microanalysis, Chalmers University of Technology, SE-41296 Göteborg, Sweden
e-mail: tholen@fy.chalmers.se

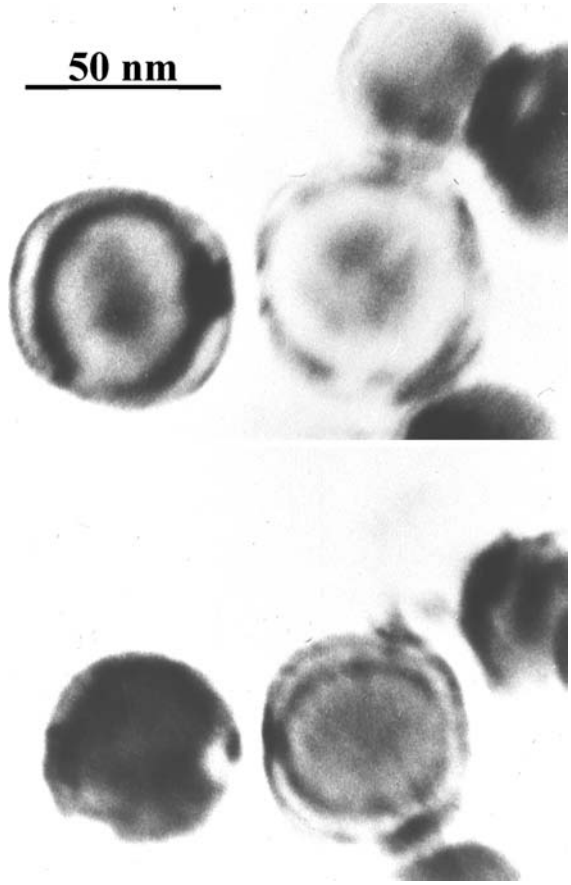

Fig. 1 Extracted Fe–Ni-particles which show stress contrast at contacts

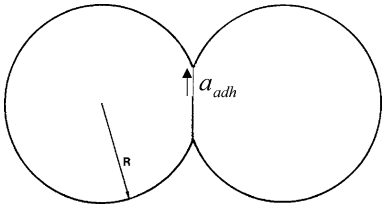

Fig. 2 Two spherical particles are making contact due to adhesion and a finite contact radius, a_{adh}, is obtained. Alternatively, an applied outside force pair, F, would also result in a finite contact radius

γ_s = surface energy (J/m^2), γ_{gb} = grain boundary energy (J/m^2), γ_{eff} = effective surface energy (J/m^2), a_{adh} = contact radius due to adhesion (m), R = particle radius (m), r = radius in the contact area (m), E = Young's modulus (N/m^2), v = Poisson's ratio, σ = normal stress at the grain boundary (N/m^2).

By inserting $v = 1/3$ and $\gamma_{gb} = \gamma_s/3$ the following expression is obtained containing the contact radius.

$$\gamma_{eff} = 0.16\frac{Ea_{adh}^3}{R^2}, \tag{3}$$

It is observed in Eq. (2) that the expression for the normal stress goes to infinity at the rim of the contact area ($r = a_{adh}$) and this is an effect of the linear theory of elasticity. This treatment has in fact the same shortcomings as the elastic description of a crack tip.

Integration of the normal stress across the contact area, however, gives zero net force. This is of course the expected result when there is no applied force.

$$\int_A \sigma \cdot dA = 0. \tag{4}$$

The maximum stress at the centre of contact is given by the following expression:

$$\sigma_{c-adh} = \frac{4Ea_{adh}}{3\pi(1-v^2)R}. \tag{5}$$

Opposite to Hertz' model there is now also required a force, F_{adh}, to separate the two particles.

$$F_{adh} = \frac{3\pi}{4}\gamma_{eff}R. \tag{6}$$

The JKR-theory can be refined so as better describe the situation at the rim of the contact, but the essential result remains. A finite contact radius is always obtained and also a force is needed to separate the particles. Alternative models have been proposed by Derjaguin et al. [4], the so-called DMT-theory and by Maugis [5] but the current experiments are at this moment not fine enough to separate the models.

In order to simulate the contrast around the contact area the displacements were first calculated by integrating the normal stress using the resulting displacement from a point force on a solid surface [6, 7]. The solving of the Howie and Whelan equations in the spheres was then done by a matrix method [8]. Some results from such calculations are shown in Fig. 3. Realistic values of the surface energy makes the contrast appear in much the same way as observed in the electron microscope which is a strong support for the theory. The surface energy can also in principle be obtained from Eq. (3). This equation is, however, very sensitive to small variations in geometry and a precise value of the surface energy is hence difficult to obtain.

A general comment on the electron microscope techniques used could be in place. An investigation of small more or less free-hanging particles is obviously a different situation than the study of thin foils. The particles are often vibrating or moving around, which makes precise diffraction experiments harder to perform. The other difficulty lies in the minute size of the particles which does not facilitate an optimal combination of imaging and diffraction. The

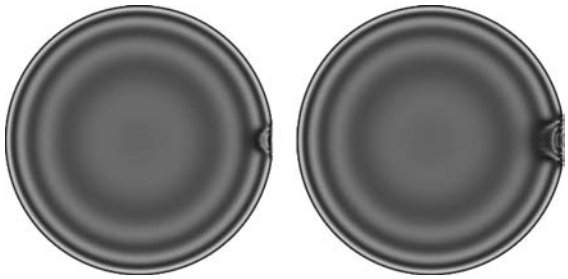

Fig. 3 Simulated electron microscope contrast based on the JKR-theory of adhesion for two particles of bcc iron in contact. The particle radius $R = 1.1 \times 10^{-7}$ m and $\gamma_s = 2.22$ J/m^2. The **g**-vector is perpendicular to the contact area. In the left figure the local radius at contact is R, in the right figure the local radius is assumed to be $2R$ just before contact

small contact between the particles is obviously an area of great interest, but requires specified diffraction conditions in the two neighbouring particles.

High-resolution, weak-beam and convergent beam diffraction techniques are difficult to use to their full potentials.

Experiments with other materials

It is essential here that the particles that meet have a clean and oxide free surface. In fact, the following discussions could equally well be applied for oxidized surfaces but the surface energy values for clean metal surfaces are better known. The clean condition for the iron–nickel particles was fulfilled by extraction as mentioned above. Presumably the magnetic force between the particles made them come together. The magnetic force itself was, however, not strong enough to cause the observed contrast phenomenon.

In the next experiment aluminium powder was used. Larger aluminium particles with an oxide coating were gently pressed against each other, the oxide scale was presumably crushed and virgin metal surfaces met. This resulted in visible stress fields both in bright field and dark field (Fig. 4). The occasional observation of stress fields in only one of two encountering particles is an effect of their different crystallographic orientation. Tilting the specimen makes fringes appear also in the neighbouring particle. Gertsman and Kwok have recently in detail investigated nanophase aluminium powder covered with an oxide layer [9].

An alternative way to obtain clean particles is by metal evaporation in a gas. The evaporation is usually done in an inert gas. The higher the gas pressure the larger the particles. The particle size also increases with the atomic number of the gas used. The evaporation here was typically done in argon with a gas pressure of 10–20 torr. The

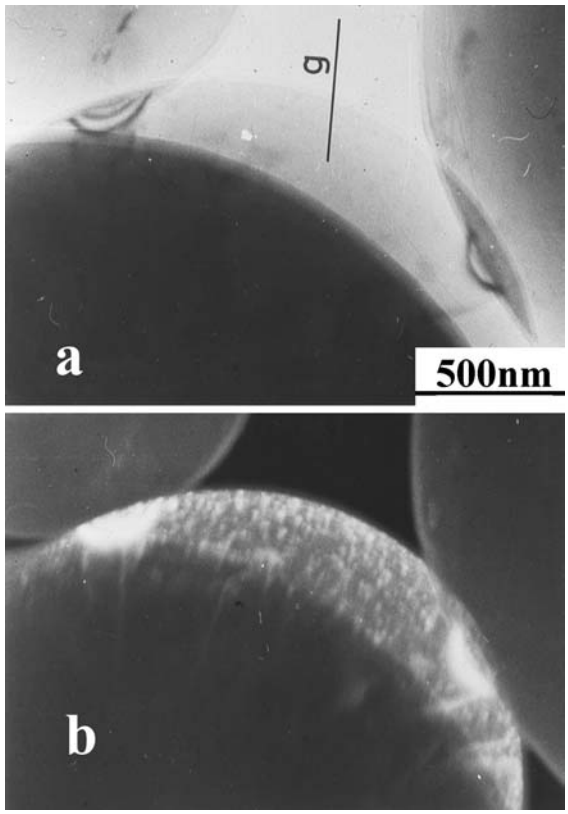

Fig. 4 Aluminium particles which show contrast at contact. The particles have been gently pressed together and the oxide scale has presumably been crushed. Electron energy 1000 keV. (**a**) Bright field. (**b**) Dark field

evaporated atoms diffuse radially out from the source through the inert gas. A certain distance out from the source, where the temperature is lower, particles form and the smoke of newly formed particles follow the convection current upwards. The whole setup bears some resemblance with a candle flame and the process is described in [10]. The smoke particles were collected on electron microscope grids covered with a holey carbon film. During the whole process the large surface of the metal smoke is exposed to the very clean gas. Accordingly the particles have very clean surfaces when they interact. The particles form branching networks as can be seen in the case of gold (Fig. 5a). It is noticed that the particles are quite similar in size (log-normal distribution). The only visible defects are twins and many of these twins emanate from the contact area. A similar result was observed for many other metals as is shown below. The TEM-studies do not actually reveal what has happened, but only the end result. As the involved stresses are very high, it is here assumed that the twins are associated with these. Another possibility could be that the twinning is taking place in order to minimize the grain-boundary energies at contact and this might also involve a thin slice of twin along the grain boundary. Any dislocation

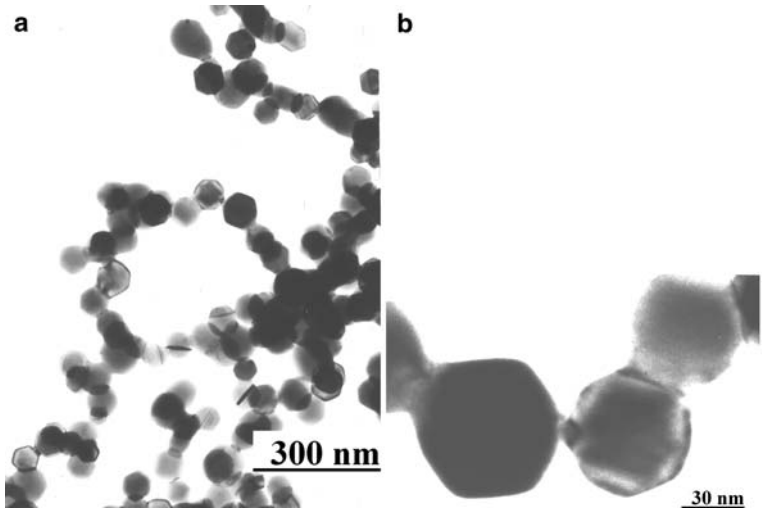

Fig. 5 Gas evaporated gold particles. (**a**) Branching network with a log-normal distribution of particle sizes. Twins are frequently observed, often in connection with contacts. (**b**) Adhesion stress field between gold particles

in the interior of a particle would, however, be forced out to the surface by image forces.

Sometimes stress fields in the contact zones of the same type as reported above were visible (Fig. 5b), but this was in fact quite a rare occasion. When two particles adhere according to the JKR-theory there is a zone in the centre with quite a high energy density. Therefore a chemical potential difference between the centre of contact and the rim is set up, which in fact is a driving force for diffusion. Due to the very short diffusion distances one would expect diffusion to occur even at quite low temperatures. Most probably many adhesion stress fields have been subjected to diffusion (a beginning sintering) and the stress fields have disappeared.

Small particles were also produced with chemical methods. Such colloidal particles of various metals have been made for a long time. The drawback with this method is, however, that the surfaces normally are not clean, which really is required for a study of adhesion. Hence this method was not pursued.

Many other metals than gold were also gas evaporated. An example with silver particles is seen in Fig. 6. Again an adhesion stress field is observed near the contacting boundary and also twins associated with the particle contact. In Fig. 7a magnesium particles with stress fields are

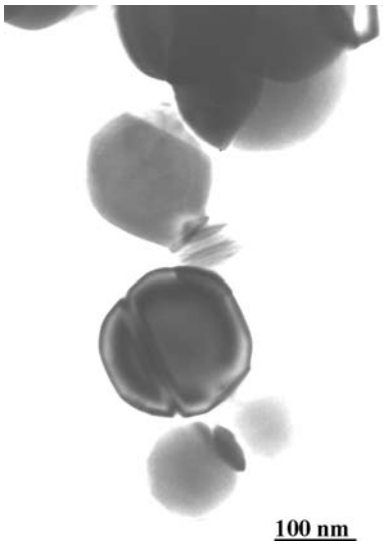

Fig. 6 Small silver particles. Twins and adhesion stress fields are shown

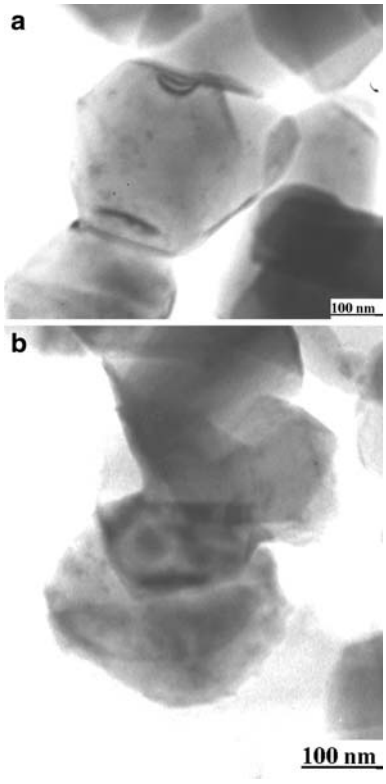

Fig. 7 (**a**) Magnesium particles with stress fields. (**b**) A stress field in the shape of a white ring is observed through two particles

shown. In Fig. 7b a ring shaped contrast fringe is seen. This observation of the contact area is done through the two particles rather than from the side as was the more frequent case.

Welding smoke is formed in much the same way as the gas evaporated particles described above, but the conditions are now more ill defined. Welding of aluminium e.g. is taking place with an inert gas but the welding smoke particles are of course oxidized afterwards. Some aluminium particles which have been collected from a welding process are shown in Fig. 8 and a stress field is observed.

Evaporated copper particles show the same branching behaviour as for example gold particles. This is in fact true for all non-magnetic particles. In Fig. 9 some copper particles are shown. Subjected to different degrees of tilt, the contrast varied. Again twins are seen associated with the contact area and stress fields are also observed.

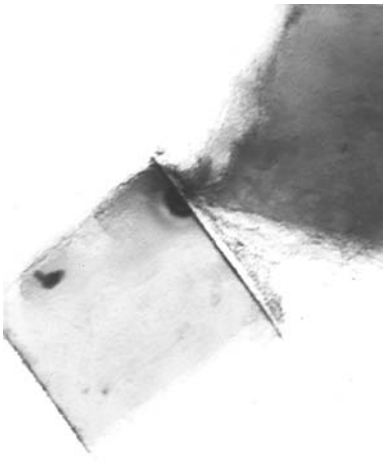

Fig. 8 Welding fume consisting of aluminium particles with an oxide layer. A stress field is observed at one of the contacts

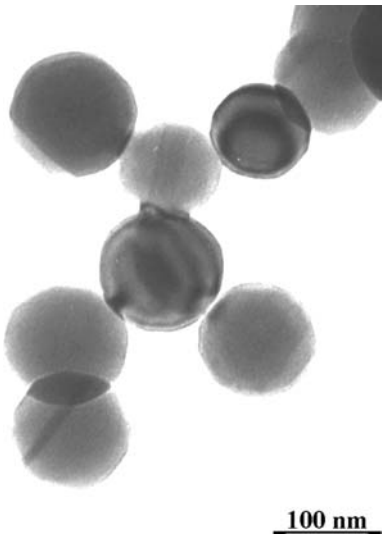

Fig. 9 Copper particles with twins and stress fields

An interesting parallel to the observation of copper nanoparticles is found in a system of larger copper particles in a powder (mean particle size 35 μm) where the individual particles had been allowed to sinter slightly. The whole system was then ground and polished (Fig. 10). Twins are observed here associated with the contact zones in much the same way as in the smaller gas evaporated particles.

When evaporating ferromagnetic material each single particle becomes a single magnetic domain (assuming that the particles are not too small to be ferromagnetic nor too big and containing many domains) and therefore the particles essentially hang together in long one-dimensional chains. Figure 11a shows some chains of cobalt particles. In each chain the particles have essentially the same size—they have a common production history. When collecting many of these chains they look like spider's web. Occasional stress fields are observed in the contact zones (Fig. 11b).

Many cobalt particles show a regular banding due to excessive twinning on one or more sets of parallel planes (Fig. 12). The structure of bulk cobalt is hcp while the equilibrium structure for small particles is fcc. This indicates that the two structures have very similar energy in small particles. A transformation between the two crystal forms requires very little energy and is martensitic in nature.

Some cobalt particle chains were also sintered in a heating stage in the electron microscope. The result was larger cobalt particles thread up regularly along a chain with larger particles like pearls on a necklace (Fig. 13). Apparently several of the original chains had sintered together each to form one bigger particle and these larger particles were evenly spread out along one chain, probably due to the magnetic forces.

The original experiment with extracted iron–nickel particles from a copper alloy [1] was repeated for a similar alloy which now instead contained coherent cobalt

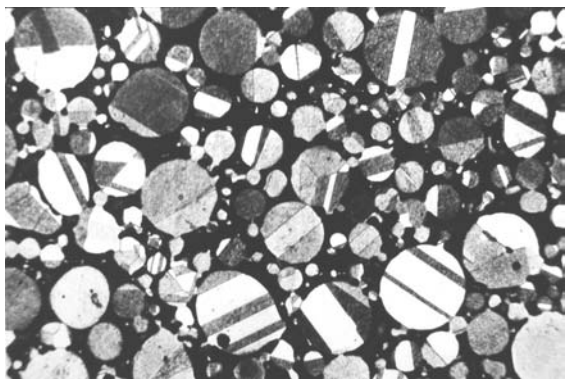

Fig. 10 Sintered larger copper particles with twins. Mean particle size is 35 μm

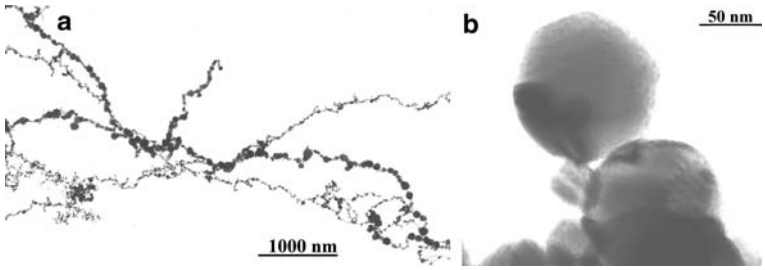

Fig. 11 (**a**) Chains of cobalt particles. (**b**) Adhesion stress field between cobalt particles. Due to diffraction effects the contrast is only visible in one of the two particles

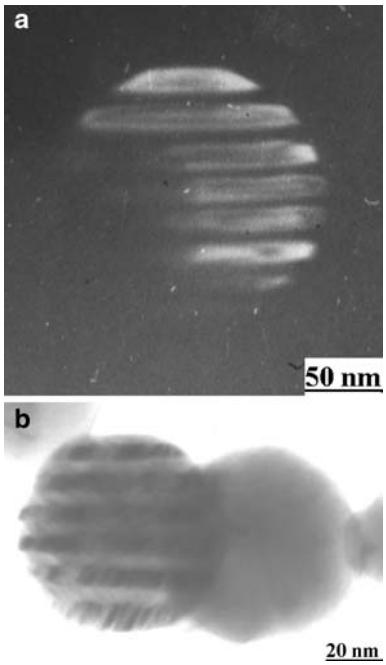

Fig. 12 Banded, regular twinned structure in cobalt particles due to a martensitic transition. (**a**) Dark field. (**b**) Twinning is observed in different planes

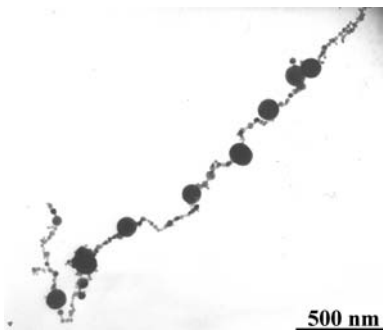

Fig. 13 Cobalt particles from different chains which have sintered and formed a very regular necklace. The magnetic force between the large cobalt particles is probably the origin of the regular structure

particles. When extracted these particles also showed abundant stress fringes at the contacting grain boundaries (Fig. 14). The particles are in fact in contact even if it does not look like that in the figure.

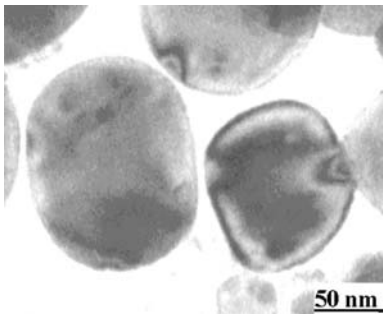

Fig. 14 Extracted cobalt particles showing stress field at contact. The particles shown are in fact in contact, even if looks differently

Magnetic nickel particles formed essentially one dimensional chains (Fig. 15). Twins were again associated with some contacts and occasional stress fields were also observed here.

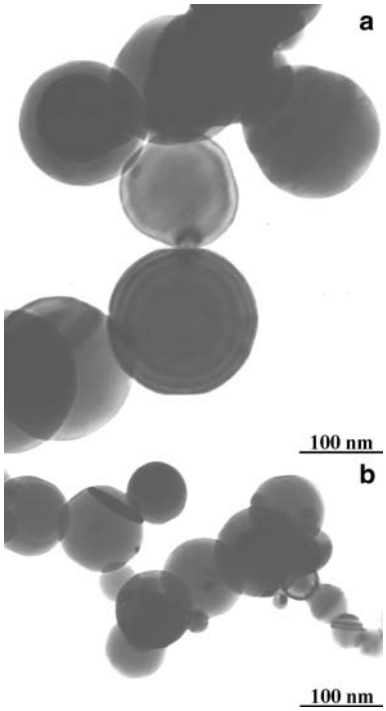

Fig. 15 Nickel particles. (**a**) Adhesion stress field at contact. (**b**) Twin starting from the edge of a contact

Possible particle vibrations

The JKR-theory describes the situation at equilibrium. But what happens from the moment when the particles first touch until they come to rest? In fact, the JKR-theory can be extended also to include this non-equilibrium stage [11]. The total energy during contacting is given in Fig. 16a as a function of a coordinate, x, which describes how the particle centres approach each other. When the particles are at their equilibrium position, $x = 0$, and the energy has a minimum. The contact radius here is of course the above mentioned radius due to adhesion.

The energy well is in fact very close to being parabolic and therefore the particles are likely to vibrate harmonically with an angular frequency ω before coming to rest.

$$\omega = \sqrt{\frac{0.78}{\rho R^2}\sqrt[3]{\frac{E^2\gamma_{\text{eff}}}{R}}}, \tag{7}$$

ω = angular frequency (rad/s), γ_{eff} = effective surface energy (J/m^2) (see above), R = particle radius (m), ρ = density (kg/m^3), E = Youngs modulus (N/m^2).

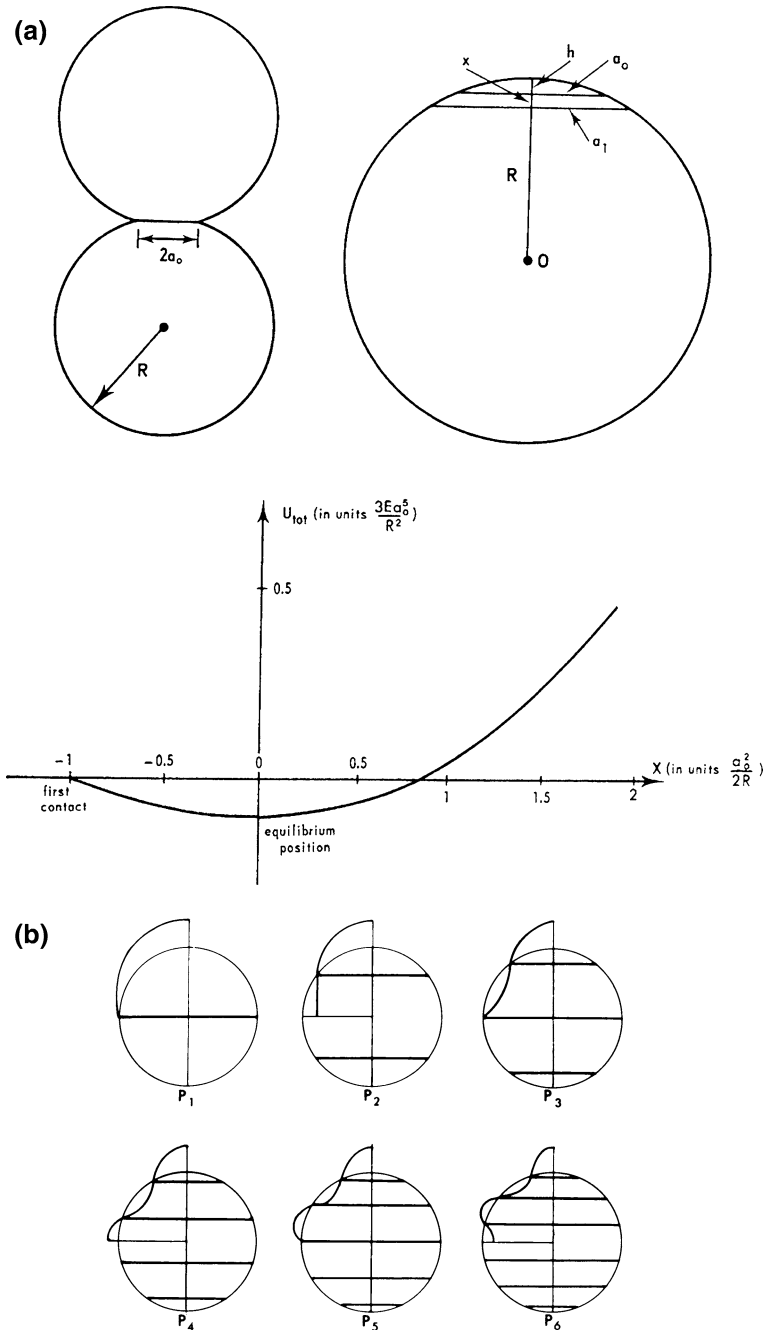

Fig. 16 Extended JKR-theory. (**a**) Upper left: The contact radius in equilibrium. Upper right: Different contact radii as a function of the distance between particle centres. Lower figure: Total energy as a function of the distance from equilibrium. (**b**) Possible vibration patterns in solid spheres

To get a feeling for the expected vibration frequencies consider particles of gold, respectively, nickel with a radius of 30 nm. This leads to an angular frequency of 1.79×10^{10} rad/s for gold and 3.58×10^{10} rad/s for nickel. The particles are thus supposed to vibrate longitudinally with a very high frequency before coming to rest.

How do these high frequencies compare and maybe couple to possible internal vibrations within the particles? We consider here four different types of vibrations namely dilational, shear, Rayleigh and capillary vibrations. Rayleigh waves are surface waves on a solid body and capillary vibrations are surface waves encountered on a liquid drop.

If we consider the same size of particles and the lowest mode of vibration the following frequencies are obtained for gold: $\omega_d = 1.16 \times 10^{11}$ rad/s, $\omega_s = 6.22 \times 10^{10}$ rad/s, $\omega_R = 5.60 \times 10^{10}$ rad/s, $\omega_c = 2.81 \times 10^9$ rad/s. For nickel the corresponding values are: $\omega_d = 2.59 \times 10^{11}$ rad/s, $\omega_s = 1.38 \times 10^{11}$ rad/s, $\omega_R = 1.25 \times 10^{11}$ rad/s, $\omega_c = 4.51 \times 10^9$ rad/s. It is noticable that these frequencies are not far off the possible longitudinal vibration frequencies at contact. The frequencies for solid bodies, however, fall above the longitudinal vibration frequencies. A coupling between longitudinal waves and internal vibrations is however a tempting possibility. Figure 16b shows some possible internal vibration patterns in spheres.

For a complete description of possible waves, Stoneley waves should also be considered.

A Stoneley wave can propagate along the interface between certain combinations of materials and it exponentially dies out from the boundary analogous to the Rayleigh waves, which only propagate near the surface. At grain boundaries in isotropic materials Stoneley waves could not exist. In anisotropic materials, on the other hand, Stoneley waves could appear along certain grain boundaries. However, some very special requirements have to be fulfilled. Two neighbouring grains are described by their two crystallographic planes which meet at the boundary and furthermore by the rotation of these grains around the common grain boundary normal. Along any such boundary, Stoneley waves can only propagate along certain directions, if they are allowed at all [12].

The riddle of the bands

The quite regular banding in cobalt particles was described above (Fig. 12). The bands consist of twins on parallel planes. Sometimes twins were also observed densely spaced on other sets of planes. The very regular twinning pattern resembles in fact a standing wave pattern. Is it possible that the longitudinal vibrations could couple to the (martensitic) transformation between the two crystal structures, fcc and hcp, resulting in internal vibrations with a high frequency?

Other models which can cause stress fringes in the small particles

Some alternative models which could cause contrast near the contacting boundary have also been investigated [13–15]. Consider first an applied force pair acting on two neighbouring particles. The obvious case to further investigate is when the two particles interact due to a magnetic force. The force between two saturated spherical magnetic particles is given by:

$$P_{\text{magn}} = \frac{8\pi}{3} \cdot \frac{B^2}{\mu_0} \cdot \frac{R^6}{x^4}, \tag{8}$$

P_{magn} = magnetic force between two spherical particles (N), B = magnetic flux density at saturation (Vs/m^2), R = particle radius (m), x = distance between particle centres (m), μ_0 = permeability of vacuum = $4\pi \times 10^{-7}$ (H/m), When the particles make contact, $x = 2R$, and

$$P_{\text{magn}} = \frac{\pi B^2 R^2}{6\mu_0}. \tag{9}$$

Using Hertz' original theory for contact between two spheres subjected to an outside force [3] it is found that the radius of contact, a_{magn}, can be written

$$a_{\text{magn}} = \left(\frac{3(1-\nu^2)P_{\text{magn}}R}{4E}\right)^{\frac{1}{3}}. \tag{10}$$

By using the expression above for the magnetic force the following contact radius is obtained

$$a_{\text{magn}} = \left(\frac{\pi(1-\nu^2)B^2}{8E\mu_0}\right)^{\frac{1}{3}} R. \tag{11}$$

The maximum stress at the centre of the contact zone, σ_c-magn, is according to Hertz given by:

$$\sigma_{c-\text{magn}} = \frac{3P_{\text{magn}}}{2\pi a_{\text{magn}}^2} = \left(\frac{B^2E^2}{\mu_0\pi^2(1-\nu^2)^2}\right)^{\frac{1}{3}}. \tag{12}$$

It is noted that the maximal stress is independant of particle radius.

The electron microscope contrast due to an applied force, P, is calculated by first considering the displacement

in the z-direction, u_z, parallel to the force. (The **g**-vector is here assumed to be parallel to the force.)

$$u_z = \frac{P}{2\pi E}\left((1+\nu)z^2(r^2+z^2)^{-\frac{3}{2}} + 2(1-\nu^2)(r^2+z^2)^{-\frac{1}{2}}\right). \tag{13}$$

The contrast is calculated along the same lines as above and the results of some calculations are shown in Fig. 18. The three particles shown have all a radius of 1.1×10^{-7} m (same as in Fig. 17) and are acted upon with three different force pairs: 2.44×10^{-8} N, 2.44×10^{-7} N and 2.44×10^{-6} N, respectively In Fig. 17 the expected force between the two particles is 2.44×10^{-8} N, which in the simulation is shown to give too low contrast. An obvious consideration is, of course, whether the magnetic field from the objective lens in the electron microscope could give rise to any further force. It turns out that as long as the external magnetic field is constant across the particles Eq. (9) is correct (if the particles originally do not have have aligned magnetic moments they will initially be subjected to a torque to put them in register). Hence we can rule out magnetic forces as the background to the stress fields. Furthermore the stress fields are also observed in non-magnetic materials.

Dislocations in the grain boundary zone

Although no dislocations (as expected) were observed in the interior of the particles due to image forces one cannot rule out the possibility of dislocations in the grain boundary plane. Although these dislocations could be of different origin we have here investigated the consequences of an edge dislocation loop lying in the boundary plane. The loop size, A, and the Burgers vector, b, were input parameters in this calculation. The displacement u_z was taken from Eshelbys expression [16] for the far field displacement from such a loop.

$$u_z = \frac{bA}{8\pi(1-\nu)r}\left((1-2\nu)\frac{z}{r} + \frac{3z^3}{r^5}\right). \tag{14}$$

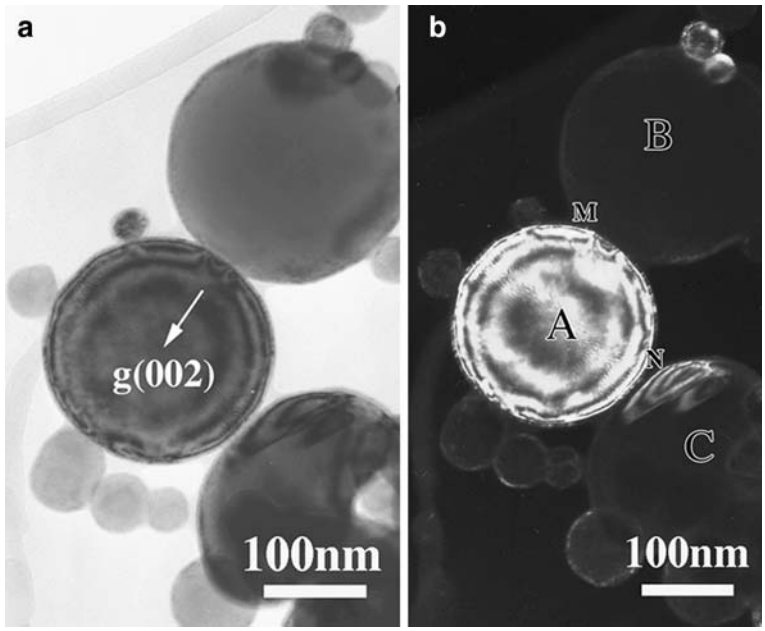

Fig. 17 Contact with stress fringes in bcc iron. (**a**) Bright-field image. (**b**) Dark-field image

Fig. 18 Simulated contrast from particles subjected to an outside force pair, F. The particle radius is 1.1×10^{-7} m. From the left the forces are $F = 2.44 \times 10^{-8}$ N, $F = 2.44 \times 10^{-7}$ N and $F = 2.44 \times 10^{-6}$ N, respectively, $E = 2.11 \times 10^{11}$ N/m^2, $\nu = 0.29$

The result of a contrast calculation from such a dislocation loop is shown in Fig. 19 for the same spheres as treated above but now with different values of bA. It is seen that the requirement for a visible contrast is that bA roughly exceeds 5×10^{-26} m^3. To get a feeling for the magnitude of this value the following example is considered. Assume that the dislocation loop takes up half the area of contact. Here the adhesion contact radius for this size of particles ($r = 1.1 \times 10^{-7}$ m) is used. Then the (dislocation) area becomes 1.93×10^{-16} m^2. In bcc iron the lattice constant is 2.86×10^{-10} m. The Burgers vector 1/2[111] equals 2.48×10^{-10} m and bA becomes 4.79×10^{-26} m^3. This is in fact very close to the excess volume in the adhesion calculations.

As in the case of adhesion the dislocation loop results in squeezed in extra material. The additional material results in an electron microscope contrast and it is difficult to distinguish the finer details of the different stress situations.

An alternative model for extra material in the grain boundary zone

There might be a different background for the boundary zone to house some extra material. Some oxide debris or some other material could exist between the two particles. This is the starting point for a new calculation of the contrast. Without knowing any details of the actual situation the stress situation is here modelled by a coherent particle in the boundary zone.

The radial dispacement in and around a coherent particle is well-known and described by the following expressions [17]

$$\begin{aligned} u(r) &= \varepsilon r & r<r_0,\\ u(r) &= \frac{\varepsilon r_0^3}{r^2} & r>r_0,\\ \delta &= \frac{2(a_1-a_2)}{a_1+a_2} & \varepsilon = \frac{3K\delta}{3K+\frac{2E}{1+\nu}}, \end{aligned} \tag{15}$$

$u(r)$ = radial displacement (m), r_0 = particle radius (m), δ = misfit between particles, a_1, a_2 = lattice parameters in particle and matrix, K = bulk modulus (N/m^2), E = Young's modulus (N/m^2), ν = Poisson's ratio.

Although the expressions above are only correct for infinite bodies they should represent a fair description of the current situation. Some examples of the expected contrast for specific situations are shown in Fig. 20. The particle radius is the same as above, 1.1×10^{-7} m. Again we have a situation with excess material in the boundary zone. When the volume of this extra material roughly exceeds 4×10^{-26} m^3 the contrast becomes visible. This is very much in accordance with the models above.

Stresses at the contact zone

The JKR theory gives the obviously wrong result that the stresses at the rim of the contact goes to infinity. However, integration of the normal stress across the contact boundary gives zero net force as expected. The normal stress at the centre of the adhesion zone gives some idea of the magnitudes involved. From Eq. (5) the stresses in Fig. 3 are calculated to be 1.0×10^{10} N/m^2 (left) and 1.2×10^{10} N/m^2 (right). The stress level is obviously very high.

In case of the magnetic force (Fig. 18 left) the stress in the centre of the contact is 2.7×10^9 N/m^2 when the magnetic force is 2.44×10^{-8} N. Obviously the stress level here is not enough to cause a visible contrast. If the external forces were larger for some unknown reason the stresses would also increase.

In case of dislocation loops the stress level has been calculated using the far field approach given by Eshelby [16] and 5×10^{-9} m from the boundary plane. The normal stresses become 2.3×10^{10} N/m^2, 4.7×10^9 N/m^2 and 2.3×10^9 N/m^2, respectively. Again it is seen that very high stress levels are associated with this model.

For coherent particles the stresses are calculated according to the following formula

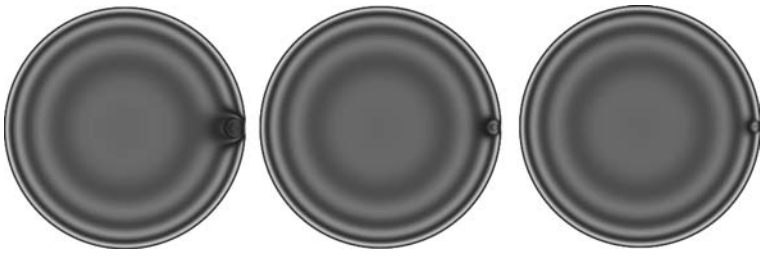

Fig. 19 Simulated contrast from an edge dislocation loop lying at the particle contact. b is Burgers vector for the loop and A its area. From the left: (**a**) $bA = 5 \times 10^{-25}$ m^3, (**b**) $bA = 1 \times 10^{-25}$ m^3, (**c**) $bA = 5 \times 10^{-26}$ m^3, respectively. The particle radius is 1.1×10^{-7} m. $E = 2.11 \times 10^{11}$ N/m^2, $\nu = 0.29$

Fig. 20 Simulated contrast from the stress field of a coherent particle lying with its centre at the contacting point between two particles. The particle radius (of the large particles) is 1.1×10^{-7} m. $E = 2.11 \times 10^{11}$ N/m^2, $v = 0.29$. From the left: $\epsilon = 5.0$; $r_0 = 2.5 \times 10^{-9}$ m, $\epsilon = 2.0$; $r_0 = 2.5 \times 10^{-9}$ m and $\epsilon = 1.0$; $r_0 = 2.5 \times 10^{-9}$ m, respectively

$$\sigma_{rr} = \frac{\mu\delta v}{\pi r^3} = \frac{\mu 4\pi\varepsilon r^3}{\pi r^3} = 4\varepsilon\mu. \tag{16}$$

The stresses in the three different simulations in Fig. 20 are 1.5×10^{12} N/m^2, 5.8×10^{11} N/m^2, 2.9×10^{11} N/m^2, respectively. The stress needed to cause a visible contrast in this case is again high, around 5×10^{10} N/m^2.

The stress levels for the various models in the centre of the contact have been calculated with the help of elasticity theory. Using the JKR-theory at the rim of the contact would yield infinitely high stresses which obviously is wrong! The very high stress levels obtained (compare with the yield stress) could indicate that one has to be a bit cautious with bulk elastic theory in such small volumes. On the other hand the high stresses seem to be necessary for the observed electron microscope contrast.

Further situations to consider

Is it possible to foresee another situation causing the contrast? Could it, for example, be possible that an oxide layer formed around the two particles after the first contact and is it possible that this oxide squeezed the particles together? The stress fields are however seen in a large number of different metals, such as are prone to oxidize and such that are not. Furthermore the model should be able to treat both magnetic and non-magnetic materials. The only model which today copes with all the situations is the original model based on adhesion.

Conclusion

In the contact zone between small particles there is sometimes observed a stress field. This is the case both for magnetic and non-magnetic particles. A model based on adhesion between the particles gives results which quite well coincide with the experiments. Other models based on an external force (e.g. magnetic), dislocations and coherent precipitates are also tested.

It is found that squeezed in material, depending on external or internal forces is common to all the models. The amount of squeezed in material essentially decides the contrast. Adhesion between particles becomes more apparent the smaller the size and is thus very important in nanotechnology.

Acknowledgement The Swedish Research Council is gratefully thanked for their support of this work. Dr. P.W. Karlsson is thanked for helpful comments.

References

1. Easterling KE, Thölén AR (1972) Acta Met 20:1001
2. Johnson KL, Kendall K, Roberts AD (1971) Proc R Soc A 324:301
3. Hertz H (1881) J Math (Crellés J) 92
4. Derjaguin BV, Muller VM, Toporov Y (1975) J Colloid Interface Sci 53:314
5. Maugis D (1992) J Colloid Interface Sci 150:243
6. Timoshenko S, Goodier JN (1951) Theory of elasticity. In: Engineering societies monographs. McGraw-Hill, New York
7. Johnson KL (1985) Contact mechanics. Cambridge Univ. Press, Cambridge, UK
8. Thölén AR (1970) Phil Mag 22(175):175
9. Gertsman VY, Kwok QSM (2005) Microsc Microanal 11:410
10. Thölén AR (1979) Acta Met 27:1765
11. Thölén AR (1980) Phys Status Solidi A 60:153
12. Thölén AR (1984) Acta Met 32(3):349
13. Yao Y, Thölén AR (2002) Nanotechnology 13:169
14. Yao Y, Thölén AR (2003) Micros Microanal 9:237
15. Thölén AR, Yao Y (2003) J Colloid Interface Sci 268:362
16. Eshelby JW (1957) Proc R Soc A 241:376
17. Ashby MF, Brown LM (1963) Phil Mag 8:1083